Alejandro Levander is an intern in the Science Undergraduate Laboratory Internship program at the National Renewable Energy Laboratory, where he is analysing high efficiency multi-junction photovoltaics. He received his undergraduate degree in materials science and engineering from Pennsylvania State University. Mr. Levander is a member of Materials Advantage. He grew up in Silver Spring, Maryland, and he enjoys backpacking, mountain biking, and traveling.

John Geisz is a senior scientist at the National Renewable Energy Laboratory (NREL). He received his Ph.D. from the University of Wisconsin in 1995, studying the application of III-V semiconductor heterostructures to optical chemical sensing. At NREL, he has specialized in epitaxial growth of III-V semiconductors by metal-organic chemical vapor deposition (MOCVD) for photovoltaic applications. He has conducted pioneering research into the growth of novel III-V semiconductor alloys containing boron or nitrogen that are lattice-matched to GaAs and silicon. Recently, he has focused more on lattice-mismatched III-V growth for the development of new high-efficiency multijunction solar cell designs.

EXAMINATION OF DISLOCATIONS IN LATTICE-MISMATCHED GaInAs/BUFFER LAYER/GaAs FOR III-V PHOTOVOLTAICS

ALEJANDRO LEVANDER AND JOHN GEISZ

ABSTRACT

Dislocations act as sites for nonradiative electron/hole pair recombination, which reduces the efficiency of photovoltaics. Lattice-matched materials can be grown on top of one another without forming a high density of dislocations. However, when the growth of lattice-mismatched (LMM) materials is attempted, many dislocations result from the relaxation of strain in the crystal structure. In an attempt to reduce the number of dislocations that propagate into a solar device when using LMM materials, a compositionally step-graded buffer is placed between the two LMM materials. In order to confine the dislocations to the buffer layer and therefore increase material quality and device efficiency, the growth temperature and thickness of the buffer layer were varied. A GaInP compositionally graded buffer and GaInAs p-n junction were grown on a GaAs substrate in a metal-organic chemical vapor deposition (MOCVD) system. A multi-beam optical stress sensor (MOSS) and X-ray diffraction (XRD) were used to characterize the strain in the epilayers. Electrical and optoelectronic properties were measured using a probe station and multimeter setup, solar simulator, and a quantum efficiency instrument. It was determined that device functionality was highly dependent on the growth temperature of the graded buffer. As growth temperature increased, so did the dislocation density in the device despite an increase in the dislocation velocity, which should have increased the dislocation annihilation rate and the diffusion of dislocations to the edge of the crystal. The thickness of the graded buffer also affected device efficiency with thinner samples performing poorly. The thinner graded buffer layers had high internal resistances from reduced carrier concentrations. In terms of efficiency, the empirically derived recipe developed by the scientists at the National Renewable Energy Laboratory (NREL) produced the highest quality cells.

INTRODUCTION

Solar power is currently used in a multitude of applications including the supplementing of household electricity, the powering of remote systems, and the generation of electricity for satellites. The development of the photovoltaic (PV) industry is critical to keeping U.S. energy dollars at home and reducing greenhouse gas emissions from coal burning power plants.

Solar cells can be made from several different materials: organic, amorphous silicon, polycrystalline II-VI, and single crystal III-V semiconductors, which are typically multi-junction. The latter is currently the most expensive to produce, but also the most efficient. The cost comes from the need for high purity chemicals and complex manufacturing processes. In space applications, where quality is the prime concern over cost, III-V multi-junction cells produced by Spectrolab and Emcore are already in use. To make multi-junction cells practical for terrestrial applications, concentrator systems are often used to focus the sunlight on a small cell, therefore reducing the cost of the cell relative to the entire system.

In general, photovoltaics made from single crystals are more efficient than those made from polycrystalline or amorphous materials. Amorphous semiconductors have a large density of dangling bonds and polycrystalline semiconductors contain grain boundaries [1]. Nonradiative electron/hole pair recombination occurs at these bulk defects, reducing the efficiency of photovoltaics made from the aforementioned materials. The superior efficiency of single crystals is caused in part by their lower density of bulk

defects. Reducing the defect density by increasing the material quality is a key method used to increase efficiency.

Single crystals of both silicon and various III-V semiconductors have been successfully produced as photovoltaics, but III-V semiconductors have certain advantageous characteristics that will make them the focus of this report. Many III-V semiconductors have a direct bandgap, high absorption coefficient, and can be produced with high-volume growth techniques, resulting in high crystalline and optoelectronic quality [2]. Depositing multiple layers of III-V semiconducting materials of differing band gap on top of each other can produce high-efficiency solar cells. Varying the band gap of the materials allows for greater absorption of the solar spectrum while minimizing thermalization of the minority carriers. Single crystal layers are epitaxially grown on top of each other using metal-organic chemical vapor deposition (MOCVD). Lattice-matched (LM) materials, materials with equal lattice spacing, can be grown on top of one another without the formation of many dislocations relatively easily. However, since lattice constant and band gap are related for III-V semiconductors, according to Figure 1, growing only LM materials limits the freedom of device design, therefore limiting theoretical efficiencies.

Having the ability to grow high quality lattice-mismatched (LMM) materials would allow the development of higher efficiency cells. Mismatch greater than 0.2% in a layer 1 µm in thickness, the "critical thickness" required to absorb most light, will result in significant dislocations and is therefore considered LMM [3]. The problem with LMM growth is that strain in the crystal results in the formation of dislocations.

Dislocations act as sites of nonradiative electron/hole pair recombination that reduce the efficiency of photovoltaics [1]. In an attempt to reduce the number of threading dislocations that propagate into the cell, a compositionally step-graded buffer is placed between the two LMM materials. Varying the chemical composition of III-V materials affects their lattice constant so simply changing the flow rates of source materials into the reactor in a stepwise fashion can generate a buffer layer between two LMM materials. LMM materials have been successfully grown at NREL with properties similar to LM materials [4]. When photovoltaic design possibilities are expanded to include LMM materials, cells with higher theoretical efficiencies can be conceived.

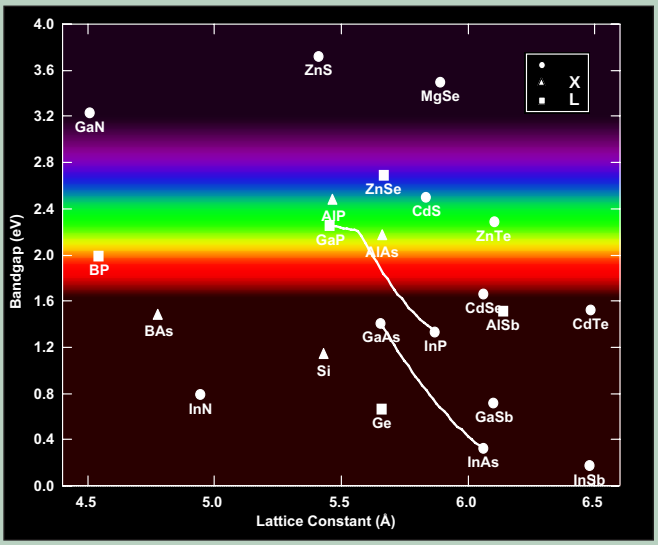

Figure 1. The relationship between chemical composition, lattice constant, and band gap for III-V semiconductors and other materials. Tie lines for the relevant materials, GaInP and GaInAs, are shown (J.F. Geisz and D.J. Friedman, "III-N-V semiconductors for solar photovoltaic applications", Semicond. Sci. Technol. v. 17, p. 769-777, (2002)).

In an attempt to grow a cell with a 1eV bandgap component, NREL has begun working on LMM growth of $Ga_{.75}In_{.25}As$ on GaAs. The two materials are LMM so a compositionally step-graded buffer must be grown between the two. GaInP was selected as the buffer layer material since it is transparent to the lower energies of light absorbed by the GaInAs bottom cell. The single-junction device examined is part of a triple junction cell composed of GaInAs (E_g = 1.0eV), a GaInP buffer layer, GaAs (E_g = 1.4eV), and GaInP (E_g = 1.8eV). This cell has the potential to reach an efficiency of more than 40% [4]. By gaining the ability to confine the dislocations formed in the buffer layer, the number of dislocations that propagate into the epilayer can be reduced. In an attempt to reduce the number of dislocations in the cell, and therefore increase material quality and device efficiency, the growth temperature and thickness of the buffer layer was examined.

MATERIALS AND METHODS

All of the cells were grown using an in-house built MOVCD reactor at atmospheric pressure with t-butylarsine, phosphine (PH_3), and triethylgallium serving as the III-V semiconductor precursors and hydrogen selenide and diethylzinc serving as dopant gases. A Zn-doped GaAs wafer with an intentional 2° miscut was used for a substrate. Before growth, the wafer was washed with an ammonia/hydrogen peroxide solution, followed by a deionized water rinse and spin-dry. The reactor was purged with arsine at 700°C prior to the growth of a 0.2µm nucleation layer of GaAs. $Ga_{.51}In_{.49}P$ was then grown LM onto GaAs as shown in Figure 2.

Eight compositionally graded LMM steps were grown as part of the Zn-doped buffer, using precisely controlled flow rates, until $Ga_{.26}In_{.74}P$ was reached. Eight steps were used in order to ensure that the mismatch between any two steps was small enough to maintain a relatively flat growth surface and a low number of dislocations. The compositional change of each step was consistent for each sample, but the step thickness varied from 0.0625 – 0.5µm to investigate the effect of that variable. In past experiments, the buffer layer thickness has been 0.25µm, but in an effort to reduce the costs associated with materials and time, the use of a thinner buffer layer was examined. In a separate experimental set, the growth temperature of the buffer was varied from 600°C – 650°C. Previous studies revealed efficiency has strong dependence on temperature, so relatively small changes from the baseline were necessary. The GaInAs cell was a 2µm thick layer of Zn-doped $Ga_{.75}In_{.25}As$, lattice-matched with $Ga_{.26}In_{.74}P$, and a 0.1µm thick layer of Se-doped $Ga_{.75}In_{.25}As$, forming a p-n junction. The active part of the device was grown at 650°C in all samples. A selenium doped window layer composed of $Ga_{.26}In_{.74}P$ and a $Ga_{.75}In_{.25}As$ contact layer were grown on top at 650°C so that photoelectrical properties could be measured.

A k-Space Associates Multi-beam Optical Stress Sensor (MOSS) mounted on the reactor recorded *in-situ* curvature measurements of

http://www.scied.science.doe.gov

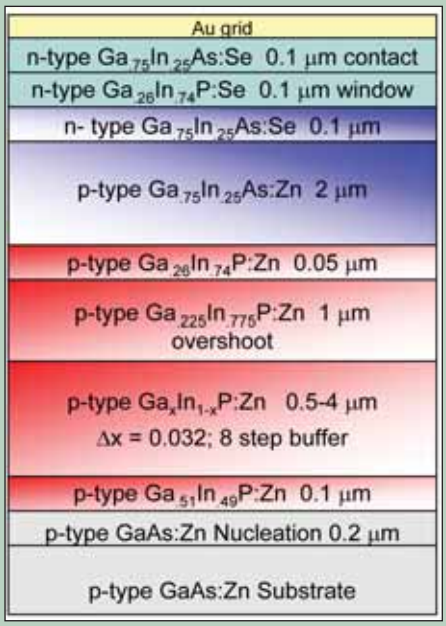

Figure 2. Schematic diagram of single-junction device grown. The temperature at which GaInP was grown and the thickness of the graded buffer were independent variables.

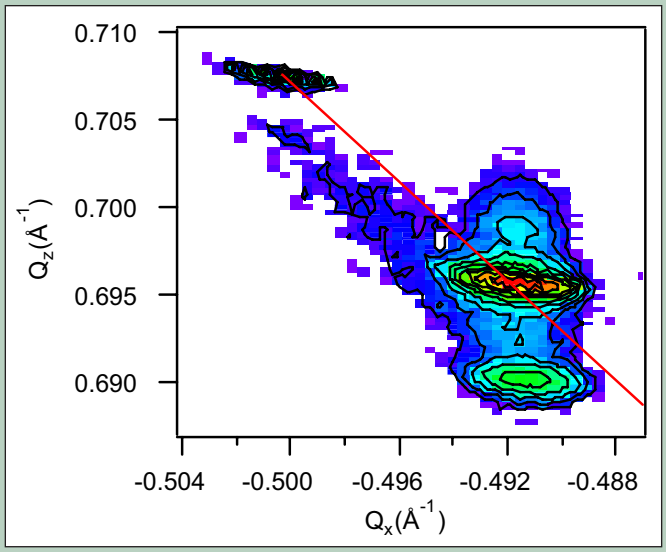

Figure 3. XRD RSM of baseline sample (620°C, 0.25µm) using the (224) glancing incidence reflection. The red line is the strain free line.

the growing crystal. The MOSS collects data using a single laser, split by an etalon into an array of nine parallel beams, which is incident on the sample. Any change in the curvature of the sample surface will result in a displacement change of the reflected lasers. This displacement change is detected by a charge-coupled device (CCD) camera, which digitizes the image and transmits the information to a data acquisition computer. The camera also detects the intensity of the laser allowing for the analysis of growth oscillations caused by wave interference.

The curvature change, Δk, is derived from the laser displacement change and is directly and quantitatively related to the strain in the sample [5]. The use of MOSS allows for the *in-situ* measurement of curvature during stress development versus an *ex-situ* measurement of the final strain in the multilayer crystal. However, the *ex-situ* technique of X-ray diffraction (XRD) is still useful for obtaining data on the tilt of the epilayer and quantitatively analyzing the strain and chemical composition of each layer. A Bede D[1] X-ray Diffractometer was used to characterize the tilt, strain, and composition of each sample. To calculate strain and composition of the epilayers, (224) grazing incidence XRD reciprocal space maps (RSM) were collected [6]. An example of a (224) RSM can be seen in Figure 3. The tilt of the epilayer was characterized by taking four (004) symmetric XRD RSMs.

Several other data sets were collected to fully characterize the quality of the cells produced. A probe station connected to a multimeter was used to measure the resistivity of the contact and window layer as well as ensure that the gold/semiconductor connection was ohmic. A modified XT-10 solar simulator from Spectrolab was used to measure I-V curves. From this data, the open circuit voltage (V_{oc}), short-circuit current (J_{sc}), fill factor (FF), and the device efficiency were derived, as well as a qualitative analysis of the internal resistance inside the cell. Quantum efficiency (QE) readings were taken using an in-house built QE instrument. QE is defined as the percentage of incident photons of a specific wavelength that generate an electron/hole pair. A scanning electron microscope was used to characterize dislocation density via electron-beam induced current (EBIC). On the EBIC image in Figure 4, the dark lines and spots represent dislocations.

RESULTS

The data is separated into two experimental groups with different independent variables: growth temperature of the graded buffer and thickness of the steps in the graded buffer. Tables 1 and 2 summarize the characterization data for the three samples including compositional and strain data gleaned from XRD as well as optoelectronic data gathered using the solar simulator.

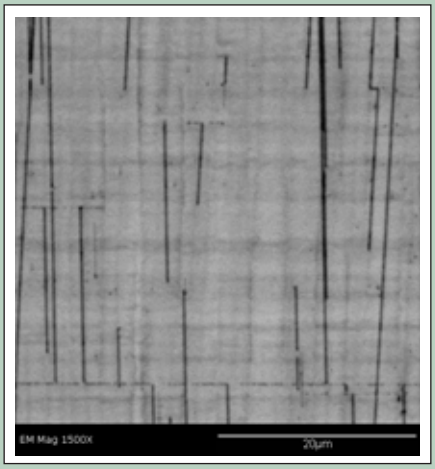

Figure 4. EBIC image of thinnest buffer layer sample (0.0625µm). Two types of dislocations appear as the darkened lines and dots.

Trends in this data are displayed in Figure 5, which includes an analysis of device efficiency, B tilt, and strain versus temperature.

The *in-situ* curvature measurements of the three growth temperatures, 600°C, 620°C, and 650°C, are shown in the same graph in Figure 6 for ease of comparison.

The cooler the growth temperature, the more compressive strain there was present in the compositionally graded buffer. The I-V and QE curves for the samples are in Figures 7 and 8 respectively.

			$Ga_xIn_{1-x}P$		$Ga_{1-x}In_xAs$		Defect Density (#x10^6/cm^2)	
Temp (°C)	A tilt	B tilt	X	Strain (%)	X	Strain (%)	Point	Line
600	0.042°	0.49°	0.220	-0.34	0.246	0.06	2.18	3.87
620	0.02°	1.2°	0.220	-0.27	0.244	0.09	4.97	3.23
650	0.032°	1.63°	0.221	-0.23	0.246	0.13%	3.33	6.45

Table 1. Tilt, composition, and strain data for the growth temperature experiment calculated using XRD RSMs.

Temp (°C)	V_{oc} (V)	J_{sc} (mA/cm^2)	FF (%)	Eff. (%)
600	0.556	16.12	77.50	6.95
620	0.547	15.00	75.70	6.21
650	0.537	13.45	26.94	1.95

Table 2. Optoelectronic data on growth temperature experiment collected using solar simulator.

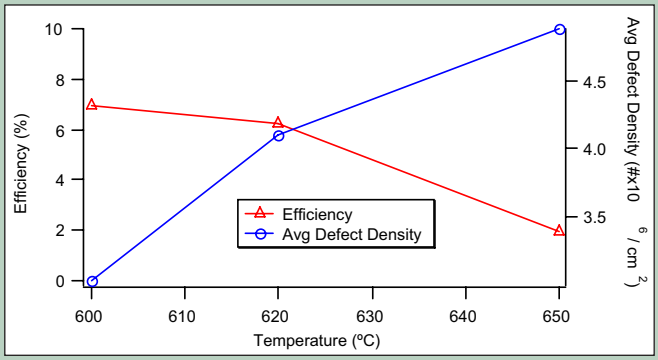

Fig. 5.A) Efficiency (%) and Avg Defect Density (#x10^6/cm^2) vs. Temperature (°C).

Fig. 5.B) B Tilt (°) vs. Temperature (°C)

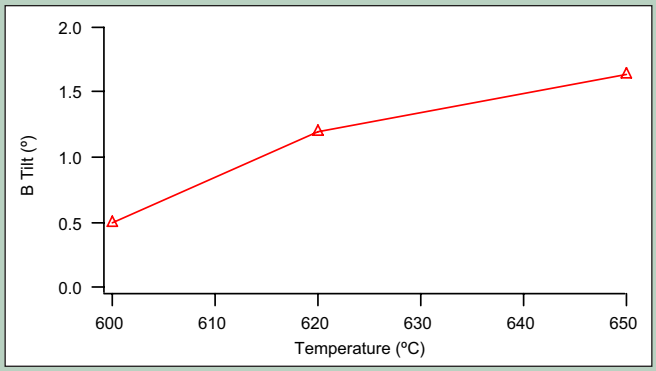

Fig. 5.C) Strain in GaInP and GaInAs (%) vs. Temperature (°C)

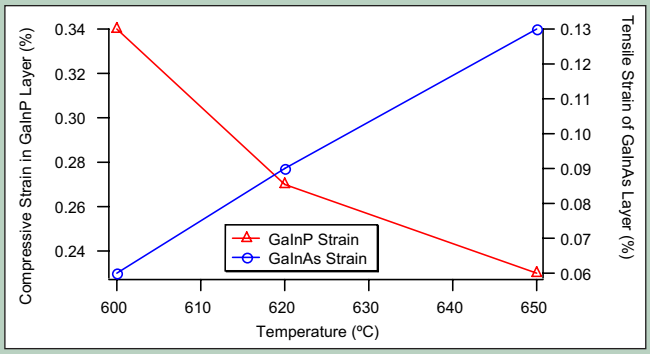

Figure 5.A-C. Several graphs showing the affect of temperature on efficiency and dislocation density (A), B tilt (B), and strain (C).

The characterization data for the thickness samples is summarized in Tables 3 and 4 with key trends highlighted in Figure 9.

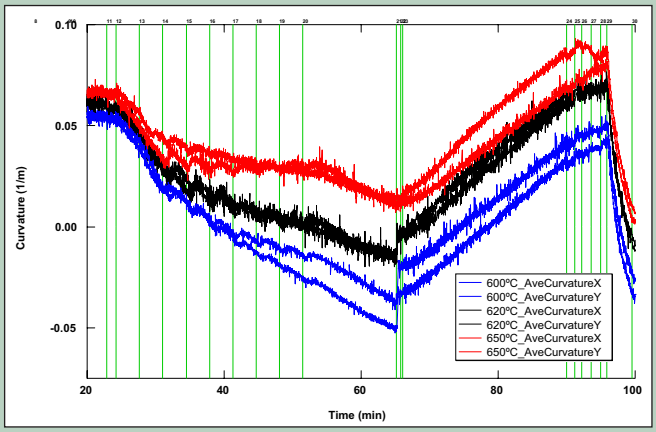

Figure 6. *In-situ* curvature measurements for the three samples in the growth temperature experiment.

The *in-situ* curvature measurements for the variable graded buffer thickness experiments are graphed separately, in Figure 10, in order to cleanly observe the strain relaxation steps in the thicker samples.

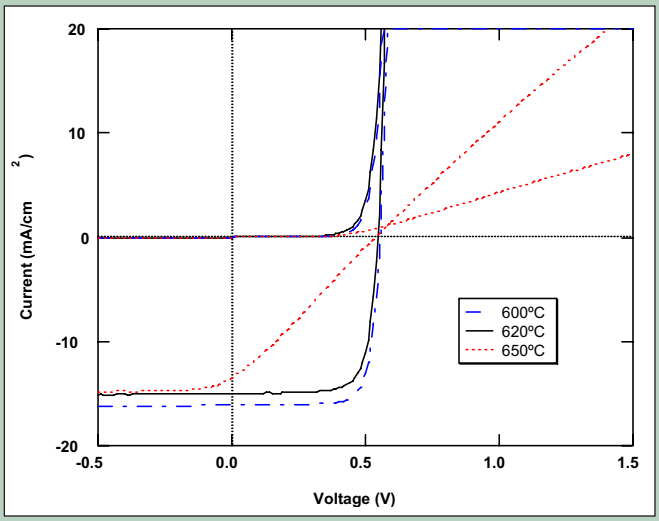

Figure 7. I-V curves of growth temperature experiment devices collected using a solar simulator.

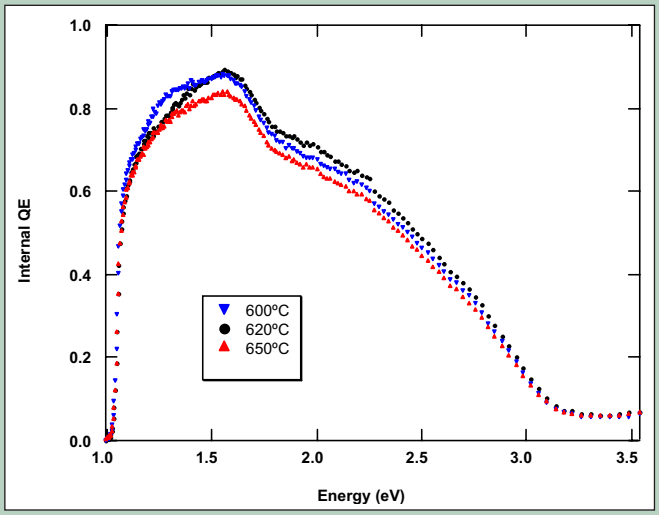

Figure 8. QE curves of the growth temperature experiment devices.

			$Ga_xIn_{1-x}P$		$Ga_{1-x}In_xAs$		Defect Density (#x10⁶/cm²)	
Step Thickness (µm)	A tilt	B tilt	X	Strain (%)	X	Strain (%)	Point	Line
0.0625	0.016°	1.66°	0.220	-0.24	0.247	0.12	3.64	1.61
0.125	0.012°	1.53°	0.220	-0.25	0.244	0.12	5.27	4.84
0.25	0.02°	1.2°	0.220	-0.27	0.244	0.09	4.97	3.23
0.5	0.006°	1.14°	0.218	-0.23	0.247	0.12	5.33	5.81

Table 3. Tilt, composition, and strain data for the graded buffer thickness experiment calculated using XRD RSMs.

Step Thickness (µm)	V_{oc} (V)	J_{sc} (mA/cm²)	FF (%)	Eff. (%)
0.0625	0.529	11.98	24.24	1.54
0.125	0.538	14.78	31.19	2.48
0.25	0.547	15.00	75.70	6.21
0.5	0.534	14.63	75.49	5.90

Table 4. Optoelectronic data on graded buffer thickness experiment collected using solar simulator.

Fig. 9.A) Efficiency (%) and Avg Defect Density (#x10⁶/cm²) vs. Step Thickness (µm)

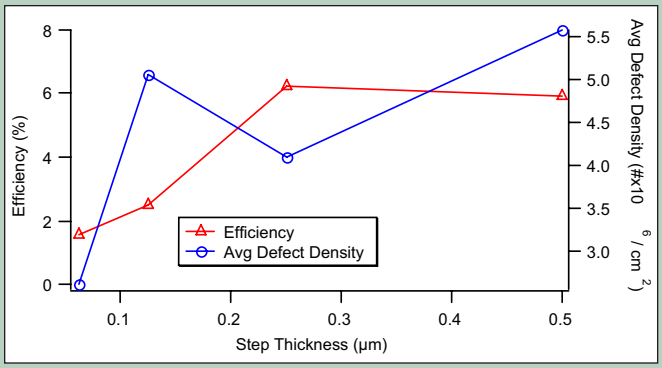

Fig. 9.B) B Tilt (°) vs. Step Thickness (µm)

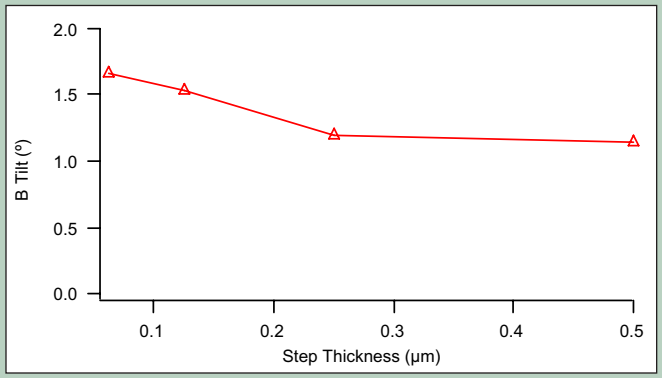

Fig. 9.C) Strain in GaInP and GaInAs (%) vs. Step Thickness (µm)

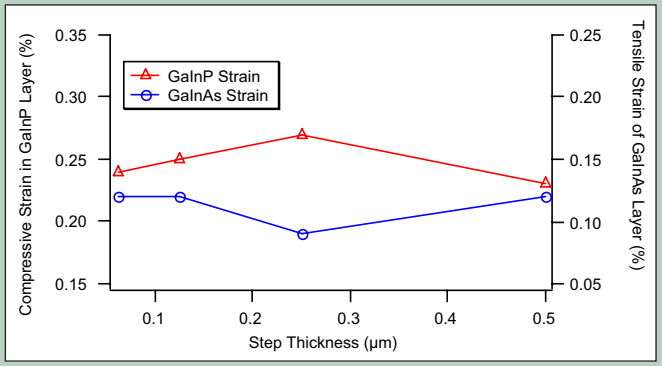

Figure 9. Several graphs showing the affect of the step thickness in the compositionally graded buffer on efficiency and dislocation density (A), B tilt (B), and strain (C).

The graphs are ordered in increasing buffer step thickness: 0.0625µm, 0.125µm, 0.25µm, and 0.5µm. Figures 11 and 12 have the I-V and QE curves for the variable buffer thickness experimental set.

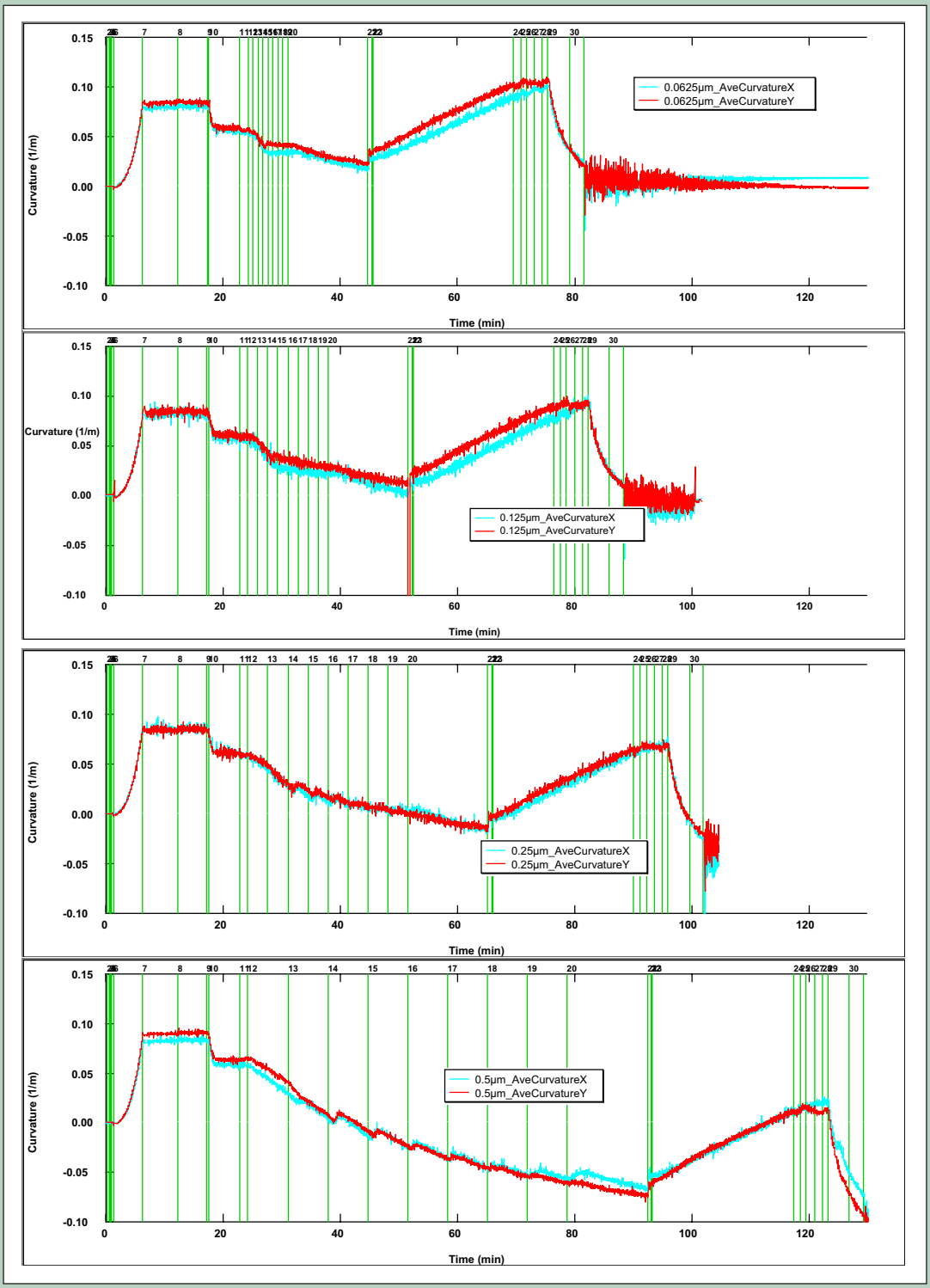

Figure 10. *In-situ* curvature measurements of the graded buffer thickness experiment samples. All of the graphs have the same scale to make qualitative examination more straightforward. The vertical lines indicate the beginning of a new stage in the growth process. The graphs are arranged in the order of thinnest buffer layer to thickest buffer layer. Deviation from the first horizontal segment is indicative of curvature in the surface. The buffer layer is grown during the segment starting near 25 min. and ends when the curvature begins to increase.

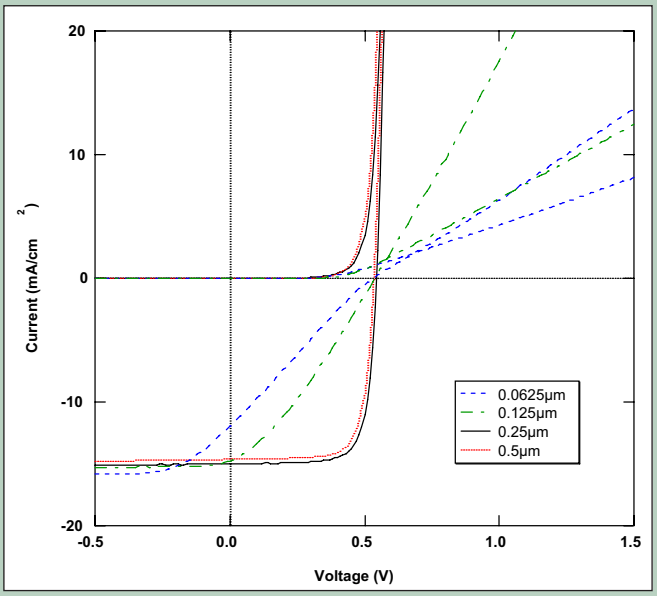

Figure 11. I-V curves of graded buffer thickness experiment devices collected using a solar simulator.

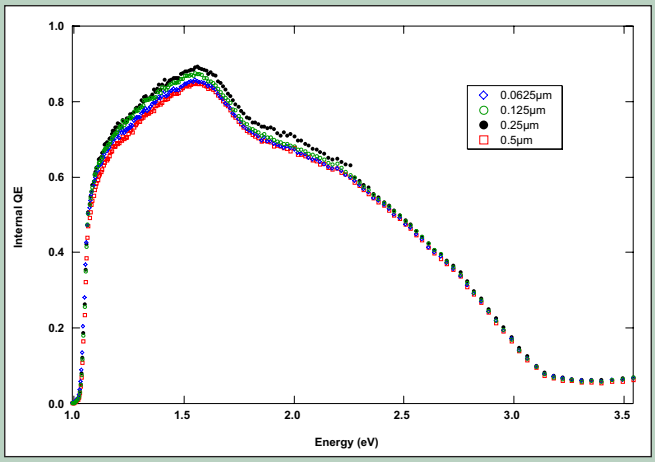

Figure 12. QE curves of the graded buffer thickness experiment devices.

DISCUSSION AND CONCLUSIONS

Temperature

Dislocations diffuse more rapidly at higher temperatures. When dislocations equal in magnitude but opposite in direction meet, they annihilate. With an increase in temperature, it was predicted that the dislocations formed during LMM growth would diffuse into each other and annihilate or diffuse to the edge of the crystal [7]. However, with higher temperatures, the formation rate of dislocations also evidently increased. This is shown in Figure 6, where the steps seen in the curvature are indicative of strain relaxation via dislocation formation. The device grown at 650°C has steps that are larger in magnitude than the steps in the 620°C and 600°C growth runs. The dislocation density increased with temperature as a result of an increased rate of formation. The predicted increase in dislocation velocity was not enough to cancel out the increased formation rate.

Other trends that exist are that B tilt increased with temperature and that as the compressive strain in the GaInP layer decreased, the tensile strain in the GaInAs layer increased. This difference in the strain is determined by the composition of the two layers, which was constant, so it was expected that if one were to decrease, the other would increase. Any increase in the compressive strain of the GaInP buffer layer was offset by less tensile strain in the GaInAs cell. Based on the efficiency data, less strain in the GaInAs cell results in higher efficiencies. The tilt of the epilayer may cause a shear stress within the crystal structure, which is another way the dislocation velocity can be increased. Again, this was not sufficient to decrease dislocation density via annihilation or diffusion to the edge of the crystal.

The I-V curves reveal that the low efficiency of the 650°C sample was partially a result of a high internal resistance. Since the ability to dope GaInP with zinc falls off sharply at a certain temperature, the resistance may be a result of insufficient doping. This occurs because zinc has a relatively high vapor pressure and is not incorporated into the lattice as easily at elevated substrate temperatures. All of the QE data for the temperature experiment was statistically similar.

Thickness

With an increase in the thickness of the buffer layer, dislocations would have more time and space to diffuse out of the crystal or annihilate. There is also an economic consideration for this variable due to the high cost of high purity III-V precursors and dopant gases. The thinnest possible buffer layer with the highest efficiency is the optimum solution. Based on the trends of the thickness experiment, there appears to be an optimum thickness for the step size near 0.25μm. At a 0.25μm step size thickness, the efficiency was highest and plateaus at greater step sizes. The B tilt remained constant. The strain in both the GaInP and GaInAs layers was unchanging with variable thickness. The MOSS data in Figure 10 reveals that the thicker buffer layer samples have more pronounced relaxation steps. These steps decrease in magnitude during growth. This may be caused by dislocations piling up and becoming pinned, preventing the formation of new dislocations. Very little curvature developed in the thinnest sample during the growth of the buffer layer. The fact that the thinnest sample had the lowest dislocation density appears anomalous since the efficiency was also the lowest. This might be caused by a factor other than defect density.

Upon examination of the I-V data, it can be concluded that thinning the buffer layer results in higher internal resistances. The high resistance could be caused by a reduction in the carrier concentration. Similar to the temperature experiment, there were no statistically significant variations in the QE data.

Based upon the presented data, several conclusions and postulates can be made. During LMM growth, strain in the crystal structure is relaxed by the formation of dislocations. As growth continues, the dislocations pile up, preventing the development of more dislocations. Higher growth temperatures allow for more strain relaxation resulting in higher dislocation densities. The added benefit of increased dislocation velocities due to a higher growth

temperature and, possibly, a larger shear stress caused by increased B tilt did not increase the rate of dislocation annihilation or diffusion to the crystal edge enough to reduce the dislocation density in the device. Growing thinner buffer layers resulted in high internal resistances, possibly caused by the buffer layer having lower carrier concentration.

Several avenues should be explored when considering the future of this project. The anomalous dislocation density of the thinnest sample should be examined using EBIC again or transmission electron microscopy. The data is sparse due to the large time commitment and high cost required for each sample. More trials should be run to increase the statistical significance of the conclusions made. Growing the graded buffer with a higher flow rate of zinc dopant may reduce the resistance at higher temperatures. The dopant type is known to have an affect on the QE of this device. Investigating the growth of a selenium doped graded buffer may prove beneficial. Selenium acts as a surfactant, tending to flatten the surface during growth. Using selenium yields poor results, but examining the curvature of a cell doped with selenium *in-situ* with the MOSS might yield relevant information relating curvature changes during growth to cell performance. Also, slightly cooler growth temperatures should be explored for the possibility of growing high quality devices with slightly higher efficiencies.

ACKNOWLEDGMENTS

This research was conducted at the National Renewable Energy Laboratory during the summer of 2006 as a part of the Summer Undergraduate Laboratory Internship (SULI). I acknowledge the United States Department of Energy, Office of Science, and NREL for creating, organizing, and funding the SULI program. I especially thank my mentor, John Geisz, for his patience, instruction, and guidance. I also acknowledge Charlene Kramer for growing my samples, Michelle Young for processing my samples, Manuel Romero for performing EBIC, and the entire III-V group at NREL.

REFERENCES

[1] Hans Joachim Möller, Semiconductors for Solar Cells, Boston: Artech House,1993.

[2] J. M. Olson, D. J. Friedman, and S. Kurtz, “High-Efficiency III-V Multijunction Solar Cells.” in Handbook of Photovoltaic Science and Engineering, Ed. A. Luque and S. Hegedus, New York City: John Wiley & Sons Ltd, 2003, pp. 359-411.

[3] J.W. Matthews and A.E. Blakeslee, “Defects in epitaxial multilayers. I. Misfit dislocations”, Journal of Crystal Growth, v.27, n.1, 1974, pp.118-25.

[4] M. W. Wanlass, S. P. Ahrenkiel, et. al., “Lattice-Mismatched Approaches for High-Performance, III-V Photovoltaic Energy Converters.” in Proceedings of the 31st IEEE Photovoltaic Specialists Conference, 2005, pp. 530-535.

[5] C. Lynch, R. Beresford, E. Chason, “Real-time Stress Evolution During Growth of $In_xAl_{1-x}As$/GaAs Metamorphic Buffer Layers.” in Journal of Vacuum Science Technology B, Vol. 22(3), May/June 2004, pp. 1539-1543.

[6] P. van der Sluis, “Determination of Strain in Epitaxial Semiconductor Layers by High-Resolution X-Ray Diffraction.” in Journal of Applied Physics, Vol. 26, 1993, pp. A188-A191.

[7] D. Hull, “Introduction to Dislocations”, 2nd ed., Pergamon Press, 1975.